The three-dimensional positron-electron momentum density study in Ge by means of a full-scale use of two-dimensional angular correlation of positron annihilation radiations

1992 J. Phys.: Condens. Matter 4 5911

(http://iopscience.iop.org/0953-8984/4/27/010)

J. Phys.: Condens. Matter 4 (1992) 5911–5920. Printed in the UK

The three-dimensional positron–electron momentum density study in Ge by means of a full-scale use of two-dimensional angular correlation of positron annihilation radiations

H Kondo, Y-K Cho‡, T Kubota, T Kawano†, K Watanabe and S Tanigawa

Institute of Materials Science, University of Tsukuba, Tsukuba, Ibaraki 305, Japan
† Radioisotope Centre, University of Tsukuba, Tsukuba, Ibaraki 305, Japan

Received 5 October 1990, in final form 16 March 1992

Abstract. The positron–electron momentum density in germanium was studied by a full-scale use of the two-dimensional angular correlation of positron annihilation radiations (2D-ACAR). The term, a full-scale use of 2D-ACAR, means that the three-dimensional momentum-space density $\rho(p)$ of the annihilation positron–electron system is directly determined from a set of experimental 2D-ACAR spectra, followed by the reconstruction technique. The obtained electron momentum density, $\rho(p)$, showed, as a whole, good agreement with the electron momentum distribution of the fully filled Jones zone with the exception that a deep dip in the origin appears, which has been observed in the 1D-ACAR or semi-2D-ACAR integrated spectra in germanium. In the present work, the electron momentum density distribution shows a ridge along the ⟨110⟩ line and a very deep valley exists along the ⟨100⟩ line, which is also the deviation from the Jones zone. In germanium, the valence 4p electrons are mainly participating in bonding σ bonds, and the distribution in space is prominently anisotropic. This anisotropy is reflected on the electron momentum density distribution in the present work. The analysis based on group theory was performed by Saito *et al* in order to investigate the origin of the anisotropy in the present work. Their results are that the anisotropy is due to the high symmetry of the crystals; they also reproduced the experimentally observed electron momentum density distribution well. It is found that the electron momentum density distribution observed by a full-scale use of 2D-ACAR provides important information on the electron states in the materials.

1. Introduction

Germanium is an elemental semiconductor and shows a typical diamond-type crystal structure, as does silicon. Its band structure is described in terms of the fully filled Jones zone. Three sets of 4p electrons form bonding σ bonds and build a covalent bond. The electronic structure of Ge has already been studied by theoretical calculations [1–3]. However, more detailed information on the electronic structure is required for a clear understanding of the relation between bands and bonds in semiconductors.

An angular correlation of positron annihilation radiation is a means to measure the electron momentum density distribution, and has been used to determine the

‡ Present address: Korea Standards Research Institute, PO Box 3, Taedok Science town, 305-6-6, Korea.

0953-8984/92/275911+10$04.50

Fermi surface of metallic materials. This method is thought to be superior to other methods (Compton scattering, de Haas–van Alphen effect, etc) in the following criteria: high resolution, high sensitivity to conduction electrons, and almost total lack of limitations on its experimental conditions (temperature, electron mean free path, atmosphere, etc). Measurements by ACAR for semiconductors, high-T_c superconductors and other materials are interesting and have been done.

The 1D-ACAR measurements for Si and Ge were performed by Erskine and McGervey [4]. The results were in good agreement with theoretical calculation [1]. 1D-ACAR and 2D-ACAR measurements for Ge were also reported [5–8]. Although the measured spectra were integrated over one or two axes, they showed, as a whole, a good agreement with the fully filled Jones zone. However, a dip was observed in the origin, which was the deviation from the Jones zone.

A clear explanation of the dip had not been given until the theoretical calculation was performed by Chiba and Akahane [9]. They calculated the positron annihilation rate based on a parameter-adjusted linear combination of atomic orbitals method. They found that some valence bands do not contribute to the annihilation rate when the photon momentum is parallel to the ⟨100⟩, ⟨110⟩ and ⟨111⟩ axes of Ge. The three-dimensional electron momentum density distribution is required in order to investigate these anisotropies.

The three-dimensional momentum density distribution is obtained from a set of 2D-ACAR spectra using the reconstruction technique. We measured the 2D-ACAR spectra for Si [10] and Ge, and reconstructed the three-dimensional momentum density distributions. The theoretical calculation was done by Saito *et al* [11] in order to clarify our results. In the present paper, the experimental results for Ge are reported and discussed.

2. Experimental details

When a positron–electron pair annihilates a two-photon emission process usually occurs. Two photons of 511 keV energy (determined by the energy conservation law) are emitted with a small angle (of the order of mrad) between their opposing directions (determined by the momentum conservation law). Since the momentum of a positron is reduced to almost zero just before the annihilation, the angle between the two emitted photons is determined mainly by the momentum of the annihilating electron. The electron momentum density is observed by measuring the angle and the coincident number of photons.

The experiments were carried out using the 2D-ACAR measurement system, which consists of a pair of detector assemblies of 128 $Bi_4Ge_3O_{12}$ (BGO) scintillators combined with 128 Hamamatsu R647 photomultiplier tubes individually and cross-slit systems [12]. The geometrical angular resolution Δ_d is 0.75 mrad × 0.75 mrad at a location of 8 m between each detector assembly and the specimen. One of the detector assemblies moves horizontally and the other moves vertically in steps of 0.2 mrad controlled automatically by programmed stepping motors. The 3×10^9 Bq ^{22}Na positron source was positioned 4 mm from the sample. A 15 kOe magnetic field was applied along the positron source–sample axis to focus the positron beam on the sample. A single crystal of Ge (n-type, $\rho = 6 \sim 7\ \Omega$ cm) was used as a sample. It was set on a copper holder connected to the cryogenic head with the (001) plane facing the positron source, and its temperature was kept at 24 K during the measurement to reduce the effect of the residual momenta of thermalized positrons.

The smearing effect caused by the thermal behaviour of a positron, Δ_t, is of the order of 0.21 mrad (FWHM) assuming the effective mass of a positron to be twice the mass of an electron. Another smearing effect, Δ_s, is due to the limited size of both the positron beam and the sample. In this case, Δ_s is determined by the positron beam size, because the size of the sample is larger than that of the positron beam, and is of the order of 0.70 mrad. The total resolutions from Δ_d, Δ_t and Δ_s are $(\Delta_d^2 + \Delta_t^2)^{1/2} = 0.78$ mrad and $(\Delta_d^2 + \Delta_t^2 + \Delta_s^2)^{1/2} = 1.05$ mrad in the directions parallel and perpendicular to the [001] axis, respectively. The measurements were performed with a step of 0.2 mrad × 0.2 mrad in the momentum range of ±22 mrad by moving both detectors.

In order to reconstruct the three-dimensional electron momentum density distribution, the measurements were performed for 10 different projection directions by rotating the sample around the [001] axis from the [100] to the [110] axis with a 5° step. The three-dimensional momentum density distribution was obtained from a set of measured 2D-ACAR spectra followed by the direct Fourier reconstruction technique.

3. Data analysis

The measured 2D-ACAR spectrum is the projection of the electron momentum density $\rho(p)$ onto the $p_y - p_z$ plane, expressed as follows:

$$N(p_y, p_z) = \int \rho(p) \mathrm{d}p_x \tag{1}$$

where p is the annihilating electron–positron pair momentum. From a set of 2D-ACAR spectra for several different projections, we can reconstruct the full three-dimensional momentum density distribution using the direct Fourier reconstruction technique [12, 13]. This technique is based on the following Fourier projection theorem [14]:

$$FT_{-2}[N(p_y, p_z)] \propto B(r)|_{x=0} = (2\pi)^{-3/2} \int\int\int \rho(p)(-ip \cdot r)\mathrm{d}p_x|_{x=0} \tag{2}$$

where $B(r)$ is the 3D Fourier transform of $\rho(p)$. The 2D-ACAR data, measured along various directions, were Fourier transformed into $B(r)$ using the 2D fast Fourier transform, followed by the interpolation of $B(r)$ onto a cubic grid. Finally, the 3D inverse Fourier transform of $B(r)$ yields the full 3D electron momentum density $\rho(p)$. The reconstruction procedure is shown in figure 1. In the reconstruction process, the resolution grows worse by more than 0.1 mrad in all directions. This kind of Fourier transformation method has a weak point in the spatial resolution; the so-called 'artifact' [15]. We adopted some special techniques to avoid this phenomenon. Firstly, we took a large angular region ±51.2 mrad, in spite of its rather small real distribution (within ±10 mrad). Secondly, the interpolation method based on third-order polynomials was adopted to enhance the spatial resolution. We examined the Fourier transformation method adopting these techniques. Some prepared three-dimensional bodies were reconstructed using this method in order to examine the relationship between the reappearance and the number of counts and directions in measurements. We could reconstruct three-dimensional bodies almost perfectly without the 'artifact' under the condition we found. (For details, see [13].)

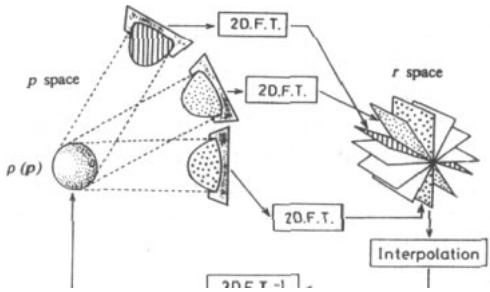

Figure 1. A schematic reconstruction procedure. 2D-ACAR spectra are projections of the electron momentum density on momentum space (p space). In order to reconstruct the 3D electron momentum density distribution, 10 spectra were measured for different directions in the present work. (In this figure, only three spectra are drawn.) The spectra are transformed (2D FT) into real space (r space). After the interpolation, the inverse transformation (3D FT^{-1}) yields the 3D electron momentum density.

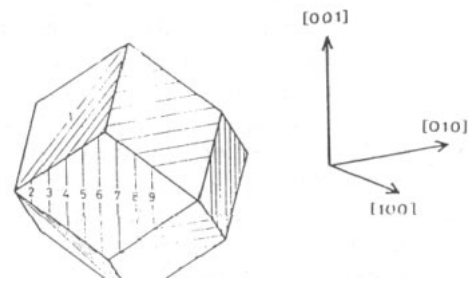

Figure 2. The Jones zone for the diamond structure, together with the three principal axes. It is a regular dodecahedron. The numbered cross sections are used in other figures and the text.

In the independent particle model, the full 3D electron momentum density $\rho(\boldsymbol{p})$ can be described as

$$\rho(\boldsymbol{p}) = \text{const} \sum_{n,\boldsymbol{k}}^{\text{occ}} \left| \int_V \mathrm{d}\boldsymbol{r}\, \psi_+(\boldsymbol{r}) \psi_{n,\boldsymbol{k}}(\boldsymbol{r}) \exp(\mathrm{i}\boldsymbol{p}\cdot\boldsymbol{r}) \right|^2 \tag{3}$$

where $\psi_{n,\boldsymbol{k}}(\boldsymbol{r})$ is the wavefunction of an electron, n is the band index, $\boldsymbol{k}$ is the wavevector, $\psi_+(\boldsymbol{r})$ is the wavefunction of a thermalized positron ($\boldsymbol{k} = 0$), V is the crystal volume and the summation is taken over all occupied electron states.

4. Results and discussion

The number of valence electrons in Ge is eight per unit cell, because there are two atoms per unit cell and four valence electrons per atom. Hence the electrons completely fill the allowed states up to the fourth band of the Brillouin zone in the reduced zone scheme. In the extended zone scheme, the Jones zone is completely filled by the electrons [16, 17]. The Jones zone scheme is shown in figure 2 with the three principal axes. It is a regular dodecahedron surrounded by {220} planes with a volume just four times as large as the volume of the first Brillouin zone.

The three-dimensional momentum density distribution in Ge, obtained by a full-scale use of 2D-ACAR, is shown in figure 3(a) as a set of several contour maps for different cross sections. Each cross section is parallel to the (100) plane and the numbers indicated in the contour maps correspond to the numbers indicated in the Jones zone scheme shown in figure 2. The vertical axis represents the momentum along the [001] direction, and the horizontal axis represents the momentum along the [010] direction in the unit of mrad.

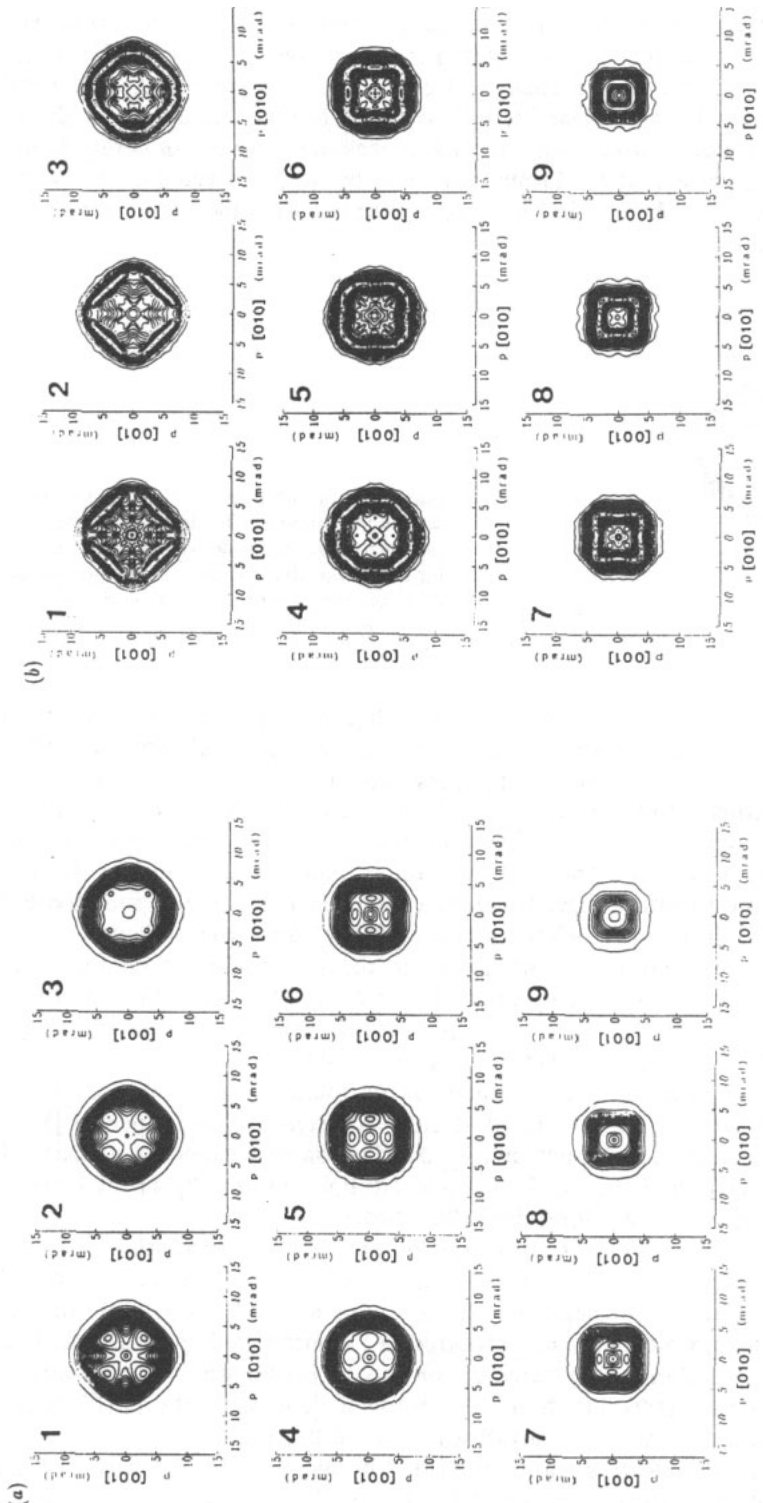

Figure 3. (*a*) The 3D electron momentum density distributions in Ge, shown as contour maps of the cross sections. The numbers in the maps correspond to the numbers in the Jones zone scheme in figure 2. The axes express the momentum in units of mrad in the [001] and [010] directions. The shape of the contour map changes gradually as the number increases. (*b*) The differentiated contour maps of the same cross sections as in (*a*). These maps help us to understand the change of the shapes.

It can be seen that the shape of the contour map for the respective cross sections changes gradually as the number indicated in the map increases. The differentiated contour maps corresponding to the contour maps in figure 3(*a*) are shown in figure 3(*b*) in order to observe the change of the shape in more detail. The outlines of the contour maps become clear. It is found clearly that the shapes of the cross sections change gradually from a square (1,2,3), passing through an octagon (4,5,6), to a 45° rotated square (7,8,9). From these results, it is ensured that the electron momentum density distribution in Ge is in agreement with the Jones zone scheme three dimensionally.

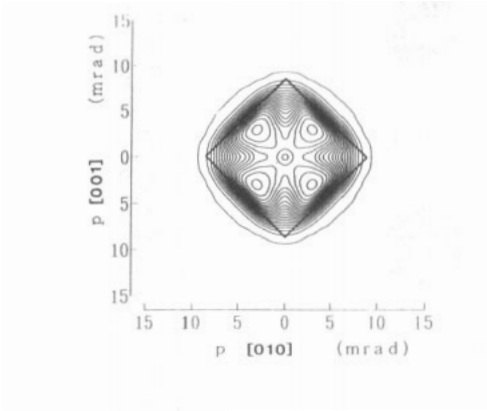

Figure 4. The enlarged contour map of the cross section numbered 1. The drawn solid lines indicate the calculated Jones zone boundaries. It is seen that the size of the obtained electron momentum density distribution agrees with that of the calculated Jones zone area.

The enlarged contour map numbered 1 in figure 3(*a*) is shown in figure 4 to compare the size of the observed electron momentum density distribution with that of the Jones zone. The corresponding cross section of the Jones zone calculated using the lattice constant of Ge ($a = 5.65$ Å) is shown by solid lines. These lines run along the regions where the contour lines are dense, except around the corner of the square. This means that the obtained electron momentum distribution also agrees with the Jones zone regarding size. It can be concluded that the electron momentum density distribution in Ge, as a whole, agrees with the Jones zone scheme.

Some characteristic structures are found in the contour maps on the electron momentum density. The low-density channels run along ⟨100⟩ directions and the dip is in the origin of the map. If the electron momentum density distribution completely agrees with the Jones zone, the electron momentum density distribution must be flat within the zone and such structures should not be found. The dip in the origin has already been reported in the integrated 1D-ACAR or semi-2D-ACAR spectra [5–8], so the dip in the electron momentum density distribution was expected to exist. It is found that the deviations from the Jones zone are not only the dip in the origin, but also the low-density channels along the ⟨100⟩ direction.

The bird's-eye view of the electron momentum density distribution is shown in figure 5, which corresponds to the cross section numbered 1 in figures 2 and 3. The height of the distribution represents the electron momentum density in arbitrary units. The dip in the origin, which had been reported in the integrated spectra, can be seen. The remarkable structure in the three-dimensional distribution is that a very deep valley exists along the ⟨100⟩ direction which forms a ridge along the ⟨110⟩ direction. Such structures are determined by a full-scale use of 2D-ACAR.

The profiles of the electron momentum density along two directions, ⟨100⟩ and ⟨110⟩, are shown in figure 6. The numbers indicated in the profiles correspond to

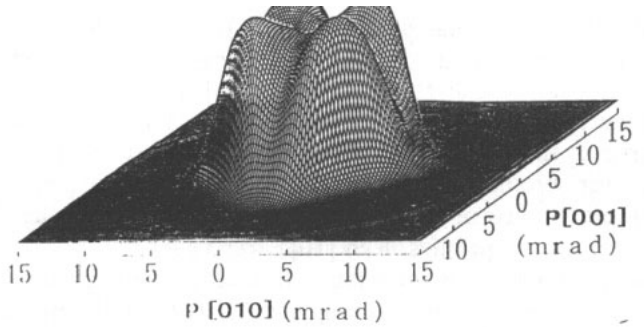

Figure 5. The bird's eye view of cross section 1. It is seen that a dip exists in the origin and a deep valley runs along the ⟨100⟩ direction.

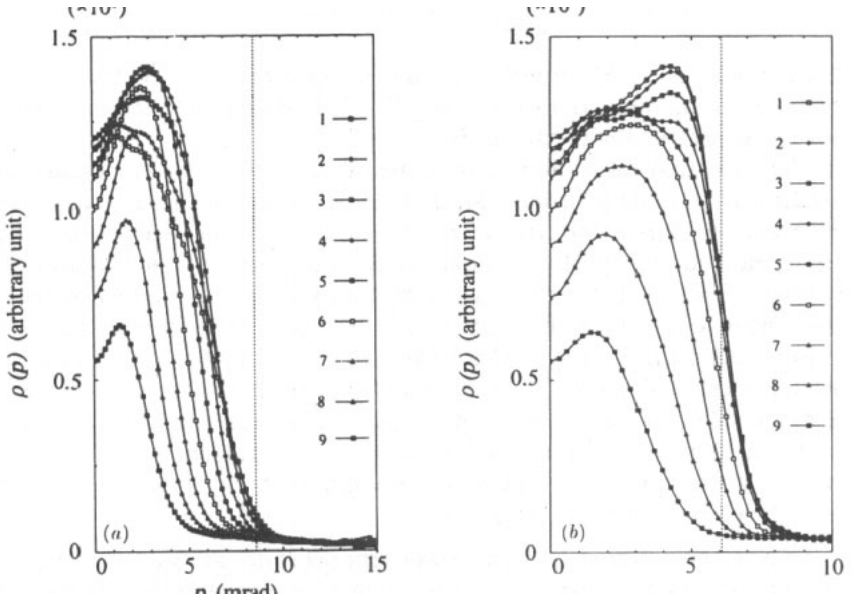

Figure 6. The profile of the electron momentum density in Ge; (*a*) along the ⟨100⟩ direction, and (*b*) along the ⟨110⟩ direction. The numbers represent the numbers of the cross sections. The origin corresponds to the Γ(000) point and the dashed line corresponds to the position of (*a*) the Γ(200) point and (*b*) the X(200) point, for profile 1.

those in the cross section. The origin corresponds to the Γ(000) point in both directions and the dashed lines correspoond to the Γ(200) point in the ⟨100⟩ direction, and the X(110) point in the ⟨110⟩ direction for the profile numbered 1. The dip is seen in the origin in both directions.

In the profiles along the ⟨100⟩ direction, shown in figure 6(*a*), the electron momentum density increases as the number increases from 1 to 5, and decreases as the number increases from 6 to 9. However, the electron momentum density simply decreases as the profile number increases along the ⟨110⟩ direction shown in figure 6(*b*). The increase in the profiles from numbers 1 to 5 along the ⟨100⟩ direction

is thought to mean that the profiles depart from the low electron momentum density channel along the ⟨100⟩ axis. Flat parts are seen in the profiles 1 and 2 along the ⟨100⟩ direction around the region from 1.8 to 3 mrad. The maximum moves to the right in profiles 1 to 3 along the ⟨110⟩ direction; this is thought to be also due to the existence of the low electron momentum density channel. Profile 1 along the ⟨110⟩ direction crosses the dashed line at the point where the slope of the profile is a maximum. However, profile 1 along the ⟨100⟩ direction is inside the dashed line. It is also due to the existence of the low electron momentum density channel. Such behaviour is also seen in the profiles in Si [10].

The anisotropy parameter ϵ is introduced to discuss the degree of the deviation from the Jones zone scheme. Profile 1 along the ⟨110⟩ direction passes through the origin of momentum space, $\Gamma(000)$, and gives a maximum value of the momentum density. The parameter ϵ is defined using this profile as follows:

$$\epsilon = \frac{\rho(p)_{\max} - \rho(p)_{\Gamma(000)}}{\rho(p)_{\max}} \times 100(\%). \tag{4}$$

It amounts to 23.0% from the profile in the present work for Ge, whereas it was reported to amount to 19% for Si [10]. This means that the magnitude of the dips for Ge is greater than that for Si.

The electron momentum density distribution of positron annihilation radiation is studied by the first-principle calculations of the annihilation rates by Saito *et al* [11] in order to explain the anisotropy observed in the present work. Their analysis is performed for the perfect crystals of Si and GaAs and for Si with neutral mono-vacancy. The result for the perfect crystal of Si can be applied to the present work. They have found three characteristics of the momentum density distribution: (i) a dip exists around the Γ point and a valley appears along the ⟨100⟩ axis; (ii) a maximum peak is located along the ⟨110⟩ axis; and (iii) the annihilation rates are nearly equal to zero outside the Jones zone. Their calculation successfully reproduces the observed electron momentum density distribution in the present work. They discussed the origin of the dip and valley based on group theory [18, 19]. The result will be introduced by quoting their paper.

'Since the positron is in the lowest-energy state, the wave function is totally symmetric; i.e. this function is invariant under any operation belonging to the symmetry group of the crystal. Therefore we obtain an important rule that, unless the electron periodic function belongs to the totally symmetric representation of the space group at a given k, the annihilation rate is zero. Thus, only functions whose representation is totally symmetric are annihilation active .... In Si, the upper two bands are annihilation inactive on the [100] line and at the Γ point because of high symmetries of the line (C_{4v}) and point (O_h), while one of the two bands is annihilation active at the other points on the (001) plane. It is concluded that the appearance of valleys along the [100] line and of the dip around the Γ point is due to the annihilation inactiveness of the upper two bands.'

In this way, the obtained electron momentum density distribution agrees with the theoretical calculation by Saito *et al* very well. It is found that the electron momentum density distribution obtained by a full-scale use of 2D-ACAR provides important information on the electronic states in the semiconductor materials.

The profiles of the autocorrelation function, $B(r)$, along the ⟨100⟩ and ⟨110⟩ directions are shown in figure 7. According to the nature of the autocorrelation

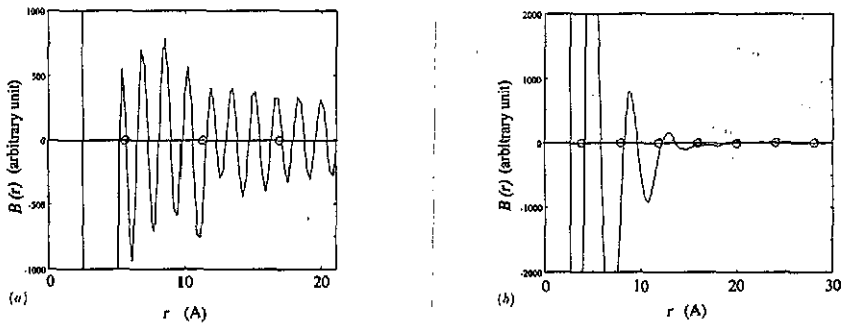

Figure 7. The profile of the autocorrelation function $B(r)$ (*a*) along the ⟨100⟩ direction, and (*b*) along the ⟨110⟩ direction. The open circles represent the lattice points of Ge.

function, $B(r)$, it is known that for filled bands $B(r)$ is zero for all $r = R$ (except $R = 0$), where R is the lattice vector of the periodic system. For the ACAR data, this is only approximately correct, even within the independent-particle model (IPM), because of the presence of the $\psi_+(r)$ [14]. So, if the IPM is valid and the effect of the presence of $\psi_+(r)$ on $\rho(p)$ is neglected, $B(r)$ should have zeros at real-space lattice points. In figure 7, the open circles represent the lattice points. It was seen that the agreement between the zeros in $B(r)$ and the lattice points is not perfect. The information of this behaviour from the experiment will be useful in understanding the effect of the positron wavefunction by comparison with the theoretical calculation.

5. Conclusion

The three-dimensional electron momentum density distribution in Ge was obtained by means of a full-scale use of 2D-ACAR. The obtained electron momentum density distribution shows a good agreement with the Jones zone scheme regarding its symmetry and size. It also shows a dip in the origin and a deep valley along the ⟨100⟩ direction; this anisotropy is the deviation from the Jones zone scheme. The theoretical calculation performed by Saito *et al* successfully reproduced the three-dimensional momentum density distribution obtained in the present work. The analysis, based on group theory, explains that the origin of the anisotropy is due to the high symmetry of the crystal. It is found that the electron momentum density distribution obtained by a full-scale use of 2D-ACAR also provides important information on the electron states in semiconductor materials.

Acknowledgments

We wish to acknowledge useful discussions with Dr M Saito and Dr A Oshiyama. This work was supported in part by a Grant-Aid for Scientific Research of the Ministry of Education, Science and Culture and by a NEDO grant for international cooperation in research. One of the authors (Cho) was also supported partly by the Korea Science Foundation.

References

[1] Stroud D and Ehrenreich H 1968 *Phys. Rev.* **171** 399

[2] Lautenschlager P, Allen P B and Cardona M 1985 *Phys. Rev.* B **31** 2163
[3] Sane A 1987 *Phys. Rev.* B **35** 5496
[4] Erskine J C and McGervey J D 1966 *Phys. Rev.* **151** 615
[5] Mayers J, McGervey J D, Walters P A and West R N 1979 *Proc. 5th Int. Conf. on Positron Annihilation* ed R Hasiguti and K Fujiwara (Sendai: Japan Institute of Metals) p 417
[6] Berko S and Mader J 1975 *Appl. Phys.* **5** 289
[7] Shulman M A, Beardsley G M and Berko S 1975 *Appl. Phys.* **5** 367
[8] West R N, Mayers J and Walters P A 1981 *J. Phys. E: Sci. Instrum.* **14** 478
[9] Chiba T and Ahahane T 1988 *Proc. 8th Int. Conf. on Positron Annihilation* ed V L Dorikens, M Korikens and O Serers (Singapore: World Scientific) p 674
[10] Cho Y-K, Kondo H, Kubota T, Watanabe K, Kurihara T and Tanigawa S unpublished
[11] Saito M, Oshiyama A and Tanigawa S 1991 *Phys. Rev.* B **44** 10601
[12] Suzuki R, Osawa M, Tanigawa S, Matsumoto M and Shiotani N 1989 *J. Phys. Soc. Japan* **58** 3251
[13] Suzuki R and Tanigawa S 1988 *Proc. 8th Int. Conf. on Positron Annihilation* ed V L Dorikens, M Korikens and O Serers (Singapore: World Scientific) p 626
[14] Berko S 1983 *Positron Solid State Physics* ed W Brandt and A Dupasquier (Amsterdam: North-Holland) p 64
[15] Cho Z H, Chan J K, Hall E L, Kruger R P and McCaughey D G 1975 *IEEE Trans. Nucl. Sci.* **22** 344
[16] Heine V and Jones R C 1969 *J. Phys. C: Solid State Phys.* **2** 719
[17] Ridley B K 1982 *Quantum Process in Semiconductors* (Oxford: Clarendon) p 6
[18] Mijnarends P E 1972 *Physica* **63** 235
[19] Harthoon R and Mijnarends P E 1978 *J. Phys. F: Met. Phys.* **8** 1147